Journal of Photochemistry and Photobiology A: Chemistry 198 (2008) 126–134

Contents lists available at ScienceDirect

Journal of Photochemistry and Photobiology A: Chemistry

journal homepage: www.elsevier.com/locate/jphotochem

Photocatalytic hydrogen evolution over mesoporous TiO_2/metal nanocomposites

Anna V. Korzhak, Natalia I. Ermokhina, Alexander L. Stroyuk*, Viktor K. Bukhtiyarov, Alexandra E. Raevskaya, Valentina I. Litvin, Stepan Ya. Kuchmiy, Vladimir G. Ilyin, Piotr A. Manorik

Pysarzhevski Institute of Physical Chemistry, National Academy of Sciences of Ukraine, 31 Nauky av., 03028 Kyiv, Ukraine

ARTICLE INFO

Article history:
Received 29 January 2008
Received in revised form 20 February 2008
Accepted 28 February 2008
Available online 6 March 2008

Keywords:
Mesoporous TiO_2
Template synthesis
Photocatalysis
Hydrogen evolution
Metals photodeposition
Metal–semiconductor nanocomposites

ABSTRACT

Na^+ complex with the dibenzo-18-crown-6 ester was used as a template to synthesize mesoporous titanium dioxide with the specific surface area 130–140 m^2/g, pore diameter 5–9 nm and anatase content 70–90%. The mesoporous TiO_2 samples prepared were found to have photocatalytic activity in Cu^{II}, Ni^{II} and Ag^{I} reduction by aliphatic alcohols. The resulting metal–semiconductor nanostructures have remarkable photocatalytic activity in hydrogen evolution from water–alcohol mixtures, their efficiency being 50–60% greater than that of the metal-containing nano-composites based on TiO_2 Degussa P25.

The effects of the thermal treatment of mesoporous TiO_2 upon its photocatalytic activity in hydrogen production were studied. The anatase content and pore size were found to be the basic parameters determining the photoreaction rate. The growth of the quantum yield of hydrogen evolution from TiO_2/Ag^0 to TiO_2/Ni^0 to TiO_2/Cu^0 was interpreted in terms of differences in the electronic interaction between metal nanoparticles and the semiconductor surface. It was found that there is an optimal metal concentration range where the quantum yield of hydrogen production is maximal. A decrease in the photoreaction rate at further increment in the metal content was supposed to be connected with the enlargement of metal nanoparticles and deterioration of the intimate electron interaction between the components of the metal–semiconductor nanocomposites.

1. Introduction

High photocatalytic activity of titanium dioxide in various redox-processes coupled with its photochemical stability and non-toxicity have stimulated the research aimed at the development of the approaches to the synthesis of TiO_2 with a special texture (i.e. surface area, porosity, spatial organization, phase composition, etc.) as well as with specified optical and electro-physical characteristics. Of great interest are also factors affecting photocatalytic properties of such titanium dioxide species and the mechanisms of the photochemical processes on the surface of porous TiO_2 materials [1–8]. Among the spatially-structurized TiO_2-containing materials the mesoporous titania seems to be the most promising candidate as a photocatalyst of effective gas- and liquid-phase photocatalytic systems [8–12]. Unique photochemical properties of the mesoporous materials originate from their high surface area, porosity, nanometer size and uniformity of the pores, small size of carcass-forming crystallites as well as a high anatase content.

There are three general approaches to the synthesis of mesoporous TiO_2-containing materials [8,10,12,13]. The first approach utilizes pre-formed TiO_2 nanoparticles, which are mixed with pore-forming agents—polymers, surfactants, viscous organic oils, etc., and calcinated at 450–500 °C. The texture of a resulting mesoporous material is therefore determined mainly by the characteristics (size, shape, size dispersion, etc.) of the initial TiO_2 nanoparticles. For example, in [14–30] the mesoporous titanium dioxide was obtained mixing TiO_2 nanoparticles with block-copolymers (from the families of Pluronic, Brij, Lutensol, Tween, etc.). Glycerol [31] and polyethylene glycol [32,33] were also successfully used as cellulating agents. The calcination of mixtures of TiO_2 nanoparticles with the pore-forming agents results in the formation of mesoporous materials with a high anatase content, specific surface area up to 200–300 m^2/g, crystallite size 5–15 nm and pore size 3–5 nm [15,16,21,26,27].

The second approach to the synthesis of TiO_2-containing mesoporous materials is based on the utilization of another mesoporous

* Corresponding author. Tel.: +380 44 525 0270.
E-mail addresses: alstroyuk@ukr.net, stroyuk@inphyschem-nas.kiev.ua (A.L. Stroyuk).

1010-6030/$ – see front matter © 2008 Published by Elsevier B.V.
doi:10.1016/j.jphotochem.2008.02.026

template—silicas, zeolites, molecular sieves, etc. [10,13,34–36] as a host for TiO_2 nanocrystals.

Finally, the third and perhaps the most versatile approach to the formation of the mesoporous TiO_2 consists in the sol–gel transition of Ti(IV) precursors in the presence of various structurized templates, mainly, surfactant micelles, vesicules, polymer nanospheres, etc. [10,13,37]. When a surfactant is used, the spatially organized template—spherical or rod-like micelles, forms on the first stage of the synthesis. The geometry and size of the micelles are determined by the surfactant concentration as well as the length and number of its hydrocarbon "tails". The hydrolysis of Ti(IV) alcoholates or other precursors in the micellar medium results in the formation of 3D inorganic carcass around the micelles. After the completion of the sol–gel transition and the gel ageing the micellar template is usually washed away with hot solvents or by the sonochemical or thermal treatment of the material. The textural parameters of the resulting highly porous material depend upon the form and concentration of the template micelles. The mesoporous titania with the specific area as high as 600 m^2/g and the pore size 2–5 nm was prepared using alkylamines and quaternary ammonium salts with long alkyl substituents [38–48], alkylphosphates [42,49], Triton X-100 [50–52], acetylacetone [53], triblock-copolymers [54–60], polyvinylpyrrolidone [61], etc. Recently, non-template syntheses of the mesoporous TiO_2 have also been reported, including sonochemical treatment of titania sols [62,63] and anodic titanium oxidation [12,64].

Due to high surface area, developed pore system and high anatase content the mesoporous TiO_2 materials often demonstrate photoelectrochemical properties and photocatalytic activity superior to those of non-porous nanomaterials, for example, TiO_2 Degussa P25 and Hombikat, which are widely used as a reference for the determination of relative photocatalytic activity of the titanium dioxide prepared by different techniques [8,9,11,65]. Mesoporous samples of TiO_2 showed high photocatalytic activity in the water reduction with the hydrogen evolution [45,61,66–70], gas-phase oxidation of ethylene and its halogen derivatives [34,71], alcohols [49,72], aldehydes [25,36,64], acetone [23,47,50,51,62,73]; liquid-phase oxidation of dyes [24,25,28,33,40–42,44,46,52,55,56,61,74,75], phenols [26,30,35,42,59,72], carbon acids [24,30,36,57,58], warfare weapon simulant—dimethyl methylphosphonate [47], potassium iodide [53], benzene [76] and toluene [43], as well as some biological toxins [48]. Thin transparent films of the mesoporous titania are of special interest due to their photoinduced superhydrophilicity [8,23,51] and perspectives of the utilization in solar cells [8,9,53,60,65,77].

The efficiency of the reductive reactions with the participation of the TiO_2 conduction band electrons, the most important one being apparently the photosplitting of water, depends strongly upon the presence of metallic co-catalysts accelerating secondary "dark" processes following the primary photochemical acts. Catalytic activity in the hydrogen photoevolution over nanostructured TiO_2 has been reported for the ultrasmall particles of Pt [1,2,8,78–82], Pd, Au [68,81], Cu [68,83], Ni [69] and some other metals [1,8].

The subject of the present paper is the photocatalytic hydrogen formation in water–alcohol mixtures with participation of metal–semiconductor nano-composites, produced *in situ* at photoreduction of copper(II) and nickel(II) chlorides and silver(I) nitrate on the surface of mesoporous TiO_2 prepared using a structure-directing template-the sodium complex with dibenzo-18-crown-6. The paper is accented on relationships between the quantum efficiencies of the photocatalytic hydrogen production and the textural characteristics of the mesoporous TiO_2 (the phase composition, surface area, porosity, etc.), nature and concentration of a metal, the composition of irradiated solutions and other parameters of the photoprocess.

2. Experimental

2.1. Materials

Reagent grade quality titanium(IV) tetrabuthoxide (TBOT), dibenzo-18-crown-6, NaCl, $CuCl_2$, $NiCl_2$ and $AgNO_3$ were obtained from Aldrich and used without additional purification. Buthanol and ethanol were distilled twice before utilization.

2.2. Synthesis of mesoporous TiO_2

Mesoporous titania was synthesized via hydrolysis of TBOT exposed to air humidity in *n*-buthanol in the presence of the sodium complex with dibenzo-18-crown-6 at the ratio TBOT:template = 5:1.

The complex Na^+-dibenzo-18-crown-6 was dissolved in *n*-buthanol at 50 °C under vigorous stirring and cooled to room temperature. A mixture of TBOT (2 vol.) with *n*-buthanol (1 vol.) was added dropwise to this solution and kept for 3 h exposed to air under stirring to achieve complete precipitation. After the sol–gel transition and ageing of the precipitate it was subjected to the hydrothermal treatment (HTT) at t_{HTT} = 100 or 175 °C for 24 h. The HTT finished the precipitate was separated from the solution, washed with ethanol and calcinated at 350 or 500 °C.

2.3. Instrumental

TiO_2 Degussa P25, containing 75% anatase [1,2], was used as a reference for the determination of the anatase content (v_a). The XRD spectra were registered on DRON-3M diffractometer operating with copper Kα-irradiation. The average size of TiO_2 crystallites ($2R$) was estimated from the broadening of the peaks in XRD spectra using well-known Scherer equation. The textural parameters (pore volume V_s and specific surface area S_{sp}) were calculated from the methanol adsorption–desorption isotherms using BET equation. The average pore diameter (D_p) was determined from the differential pore size distribution curves. In the section describing the photocatalytic experiments, the following labelling of TiO_2 samples was adopted: $TiO_2(t_{HTT};t_{calc})$, where t_{calc} is the calcination temperature.

The structure of mesoporous TiO_2 samples was studied using the scanning electron microscope (SEM) JEOL JSM-840 with the add-on device for X-ray microanalysis LINC and the transmission electron microscope (TEM) Phillips EM-400T with the accelerating voltage 80 kV.

The photocatalytic hydrogen evolution was studied in a temperature-controlled 10 mL glass reactor with magnetic content stirring. The reactors were illuminated by a 1000 W mercury high pressure lamp in the narrow spectral window 310–370 nm with the peak intensity at λ_{max} = 365 nm or by unfiltered light at $\lambda > 310$ nm. Solutions were evacuated prior to the irradiation. Photocatalytic systems were typically composed of 10 mL water–ethanol mixture (5 vol. water and 95 vol. ethanol), 0.05 g TiO_2, 0.02 g Pd/SiO_2 or a $(0.5–5.0) \times 10^{-4}$ M metal salt ($CuCl_2$, $NiCl_2$ or $AgNO_3$). Co-catalyst Pd/SiO_2 was prepared reducing $PdCl_2$ (0.2% of the carrier mass) on the surface of a commercial silica by hydrogen in an alcohol solution. The volume of hydrogen evolved was measured on a gas chromatograph.

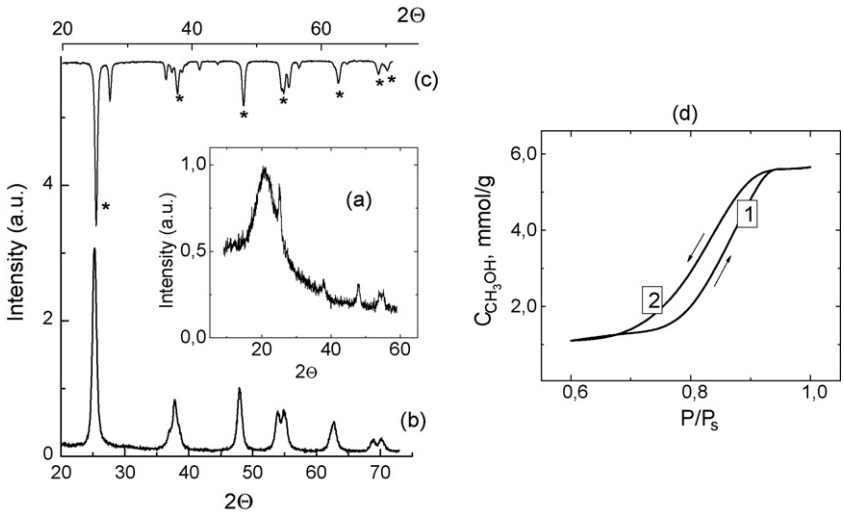

Fig. 1. (a–c) XRD patterns of TiO_2 synthesized under various conditions (a, b), and TiO_2 Degussa P25 (c). The sample (a) was not exposed to HTT and was only calcinated at 500 °C, the sample (b) was exposed to HTT at 175 °C and then calcinated at 500 °C. The anatase reflexes are denoted by an asterisk. (d) Methanol vapor adsorption (curve 1) and desorption (curve 2) isotherms on the mesoporous TiO_2(100;350).

3. Results and discussion

3.1. Characterization of mesoporous TiO_2

It was found that TBOT hydrolysis and sol–gel transformation in the presence of Na^+-dibenzo-18-crown-6 complex produces amorphous titanium dioxide. The calcination of the amorphous TiO_2 at 500 °C results in crystallization of the sample (Fig. 1a) and development of a porous structure with rather high specific surface area (up to 90 m^2/g) and the average pore diameter 5.0 nm (Table 1, sample No. 2).

The HTT of oxide materials in aqueous solutions at 100–200 °C is nowadays the widely used technique for increasing of the crystallinity of micro- and mesoporous materials avoiding deterioration of their 3D frame structure [84]. This makes the HTT a powerful method for improvement of the crystallinity of the pore walls in mesoporous TiO_2 samples without their deformation and collapse as is often the case at high-temperature calcination of such materials [15,85,86].

It was further found that a combination of HTT of TiO_2 samples with the following calcination at 350 or 500 °C results in even more complete crystallization of the primary amorphous oxide yielding mesoporous materials with specific surface area greater than 100 m^2/g, pore diameter 7–10 nm and TiO_2 crystallite size 9–10 nm (Table 1, samples No. 3–5). Fig. 1b demonstrates the XRD spectrum of mesoporous TiO_2 sample after the HTT at 175 °C and calcination at 500 °C, i.e. TiO_2(175;500). Comparison of the position and intensity of the XRD peaks of the mesoporous sample with those of TiO_2 Degussa P25 (Fig. 1c) showed that the anatase content in the mesoporous material is as high as 90% (Table 1, sample No. 5).

Fig. 1d shows a methanol adsorption–desorption isotherm of the mesoporous titanium dioxide TiO_2(100;350). Methanol was used as a model adsorbate to determine the textural characteristics of the mesoporous material in conditions close to those used in the photocatalytic experiments. The shape of the isotherm, as well as a H1 type hysteresis between the adsorption and desorption isotherms, are typical for mesoporous materials [14,15,23,38,49,62].

The mesoporous character of the synthesized TiO_2 materials was further confirmed by the results of electron microscopy study. The TEM image of TiO_2(175;500) given in Fig. 2a shows that the sample is composed of separate loosely aggregated 8–10 nm TiO_2 nanoparticles which is in good agreement with the XRD results. All reflexes in the electron diffraction patterns of TiO_2(175;500) were identified as belonging to anatase (inset in Fig. 2a). The SEM and TEM images presented in Fig. 2 evidence that mesoporosity and high surface area of the material under discussion arise from the formation of frame structures by separate TiO_2 nanocrystallites.

Data presented in Table 1 show the general tendency of the growth of anatase content as well as pore volume and diameter at an increase in the temperature of both the HTT and the calcination.

3.2. Photocatalytic hydrogen evolution with participation of the mesoporous TiO_2

No noticeable amounts of hydrogen was produced at the irradiation of suspensions of the mesoporous TiO_2 without Pd/SiO_2 or other metal salts. Instead, the TiO_2 suspension was gaining

Table 1
Variation of the textural parameters and the quantum yield of the photocatalytic hydrogen production $\Phi(H_2)$ in the presence of $[NiCl_2] = 1 \times 10^{-4}$ M at different conditions of preparation of the mesoporous TiO_2

No	Sample	t_{HTT} (°C)	t_{calc} (°C)	V_S (cm^3/g)	S_{sp} (m^2/g)	D_p (nm)	2R (nm)	v_a, (%)	$\Phi(H_2)$
1	Amorphous TiO_2	–	–	–	–	–	–	0	0
2	TiO_2(–;500)	–	500	0.17	90	5.0	8.6	30	0.04
3	TiO_2(100;500)	100	500	0.21	96	7.2	9.4	75	0.20
4	TiO_2(175;350)	175	350	0.42	141	7.2	9.0	70	0.20
5	TiO_2(175;500)	175	500	0.45	130	9.2	9.7	90	0.38
6	*Degussa* P25	–	–	–	50[a]	–	24.0[a]	75[a]	0.21

[a] From Ref. [1].

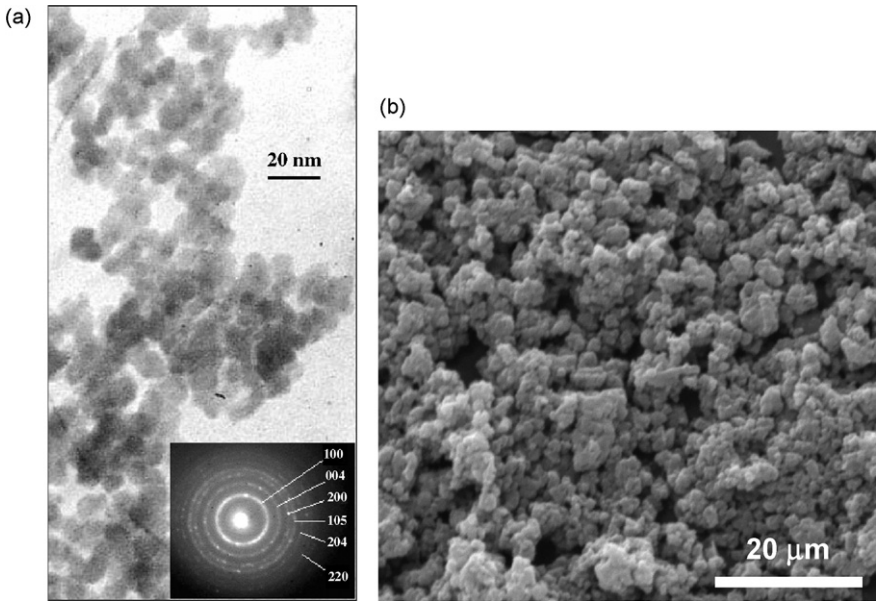

Fig. 2. TEM (a) and SEM (b) images of the mesoporous TiO_2(175;500). Inset in subpart (a): electron diffraction pattern of the mesoporous TiO_2 with the corresponding plane indices.

grey-blue at the irradiation. The photoinduced coloration of mesoporous TiO_2 indicates accumulation of Ti^{III} in the semiconductor grains takes place as a result of Ti^{IV} reduction by the photogenerated conduction band electrons [4,87–90]:

$$TiO_2 + h\nu \rightarrow TiO_2(e_{CB}^- + h_{VB}^+) \quad (1)$$

$$Ti^{4+}O_2 + e_{CB}^- \rightarrow Ti^{3+}O_2 \quad (2)$$

$$h_{VB}^+ + CH_3CH_2OH \rightarrow CH_3CH_2^{\bullet +}OH \rightarrow H^+ + CH_3CH^{\bullet}OH \quad (3)$$

where $h\nu$ is an absorbed light quantum, e_{CB}^- and h_{VB}^+ are the conduction band electron and valence band hole, respectively.

The $CH_3CH^{\bullet}OH$ radicals can, in turn, inject electron into the conduction band of TiO_2, converting to acetaldehyde (reaction (4)) [1,2]:

$$CH_3CH^{\bullet}OH + TiO_2 \rightarrow (e_{CB}^-)TiO_2 + CH_3CHO + H^+ \quad (4)$$

This phenomenon points at a small rate of reactions between the photogenerated electrons and H_2O or C_2H_5OH in cases when no additional charge transfer mediator is present in the photocatalytic system [1,4,87].

The capability of mesoporous TiO_2 to accumulate Ti^{III} under the illumination, which can be observed visually and was earlier confirmed by EPR data [91], sharply distinguishes these materials from conventional non-porous nanocrystalline TiO_2 materials, for, example, Degussa P25 or Hombikat. It also results in some specifics of the photocatalytic behavior of the mesoporous titanium dioxide in hydrogen evolution. According to [91], the photocatalytic systems containing mesoporous TiO_2 and Pd/SiO_2, can produce additional amounts of molecular hydrogen when kept in dark some time after the termination of the illumination. The post-illumination reaction is connected with gradual reduction of water molecules by Ti^{III} species. It was concluded from this fact [91] that a fraction of the photogenerated conduction band electrons gets captured in the form of Ti^{III} on the developed inner pore surface of the mesoporous TiO_2 and, probably, on the boundaries between the nanocrystallites. The captured charge carriers migrate slowly to the outer surface of the photocatalyst where they can transfer to Pd/SiO_2 and participate in the water reduction. Therefore, to improve the efficiency of the photocatalytic hydrogen evolution one should try to introduce the metallic co-catalyst directly into the pores of mesoporous TiO_2. This goal can be logically achieved at the photocatalytic reduction of some metals on the surface of TiO_2.

When the photocatalytic systems containing $CuCl_2$, $NiCl_2$ or $AgNO_3$ instead of Pd/SiO_2 are illuminated, rapid darkening of mesoporous TiO_2 is observed along with the evolution of molecular hydrogen. No changes in TiO_2 color take place when these systems are kept in dark. Air admission into pre-irradiated solutions results in decoloration of the photocatalyst and termination of hydrogen formation. With regard to these observations it was concluded that the photoinduced darkening of the mesoporous TiO_2 is caused by the photocatalytic deposition of dispersed metal particles onto its surface. The lack of solution coloration after complete sedimentation of the irradiated photocatalyst indicate that metal photoreduction occurs only on the surface of TiO_2 and not in the solution around it. High rate of the air oxidation of photodeposited metal indicates that the photocatalytic reduction produces ultrasmall highly reactive metal nanoparticles on the semiconductor surface.

The flat band potential of TiO_2 is $E_{fb} = -0.14$ V (rel. to normal hydrogen electrode, NHE) [1] at pH 0 and increases by 59 mV per pH unit. In water–ethanol solutions, one can assume pH to be close to 7 and $E_{fb} \approx E_{CB} = -0.55$ V. Redox potentials $E(M^{z+}/M^0)$ of copper(II), nickel(II) and silver(I) are 0.34, −0.25 and 0.80 V, respectively. Comparison of these potentials with $E_{CB}(TiO_2)$ shows that the photocatalytic reduction of all three metals by the TiO_2 conduction band electrons is favourable until complete conversion of the dissolved metal salts. For example, in the case of nickel(II) having the most negative redox-potential of all three metals, $E^{\circ}(Ni^{2+}/Ni^0)$ changes from −0.25 to −0.40 V (NHE) at 99% Ni(II) conversion [92]:

$$2Ti^{3+}O_2 + Ni^{2+} \rightarrow 2Ti^{4+}O_2/Ni^0 \quad (5)$$

$$TiO_2/n(Ni^0) \rightarrow TiO_2/Ni_n{}^0 \quad (6)$$

The photodeposited metals (M = Cu, Ni, Ag) can act as nano-sized electrodes [1,93], accumulating the photogenerated TiO_2 conduction band electrons, diminishing the water reduction overvoltage and accelerating recombination of the hydrogen atoms:

$$TiO_2(e_{CB}^-)/M_n{}^0 \rightarrow TiO_2/M_n{}^0(e^-) \quad (7)$$

$$TiO_2/M_n{}^0(e^-) + H_2O \rightarrow TiO_2/M_n{}^0(H^{\bullet}) + OH^- \quad (8)$$

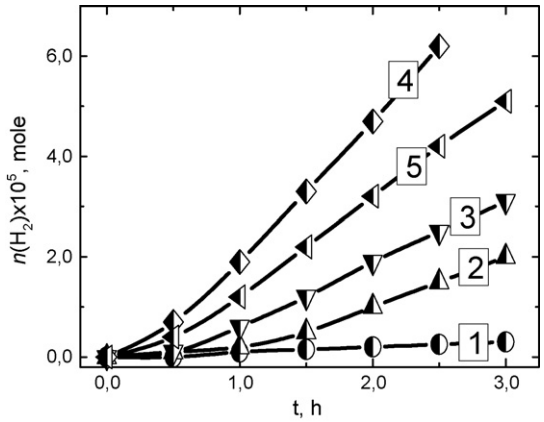

Fig. 3. Kinetic curves of the photocatalytic hydrogen evolution from the water–ethanol mixture in the presence of TiO_2/Ni_n^0 nanocomposites prepared from mesoporous TiO_2 (curves 1–4) and Degussa P25 (curve 5). The TiO_2 sample used was 1—TiO_2(–;500), 2—TiO_2(100;500), 3—TiO_2(175;350), 4—TiO_2(175;500). $[NiCl_2] = 1 \times 10^{-4}$ M, 40 °C, $I = 1.3 \times 10^{-6}$ Einstein/min.

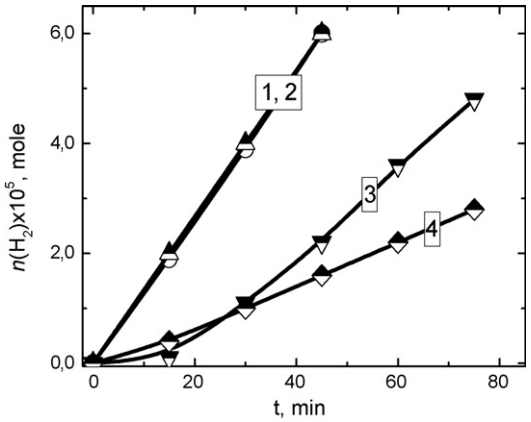

Fig. 4. Kinetic curves of the photocatalytic hydrogen production from a water–ethanol mixture in the presence of the mesoporous TiO_2(175;500) and Pd/SiO_2 (1), $CuCl_2$ (2), $NiCl_2$ (3), $AgNO_3$ (4). Metal concentration -2×10^{-4} M, 40 °C, $I = 1.3 \times 10^{-6}$ Einstein/min.

$$TiO_2/M_n^0(2H^\bullet) \rightarrow TiO_2/M_n^0 + H_2 \quad (9)$$

3.2.1. Effect of the thermal treatment conditions on the photocatalytic properties of the mesoporous TiO_2

It was found that the photocatalytic activity of mesoporous titania in the hydrogen production in the presence of either Pd/SiO_2 or photocatalytically deposited Cu_n^0, Ni_n^0 and Ag_n^0 nanoparticles depends substantially on the history of the oxide sample preparation, mainly on the HTT and calcination temperatures. One of such dependences is presented in Table 1 and Fig. 3 for *meso*-TiO_2/Ni_n^0. Amorphous titanium dioxide, prepared without post-synthesis thermal treatment, was found to be inactive in both photocatalytic metal reduction and hydrogen evolution (Table 1, sample No. 1). A sample calcinated at 500 °C without the preliminary HTT (sample No. 2) showed low photoactivity. Only a combination of the HTT at 175 °C and the calcination at 500 °C resulted in mesoporous material with the photocatalytic activity in water reduction comparable to that of commercial TiO_2 Degussa P25. Fig. 3 presents kinetic curves of the photocatalytic hydrogen evolution from a water–ethanol mixture containing $NiCl_2$ and mesoporous TiO_2 samples with different history as well as TiO_2 Degussa P25. As can be seen from the figure, there is some acceleration of hydrogen production on the initial stage of the photoreaction (0.5–1.0 h) accounted for by the nickel nanoparticles formation. After complete metal photodeposition the hydrogen evolution rate achieves a constant value and does not change at hours-long illumination.

Table 1 shows that the most significant factors affecting the photocatalytic activity of mesoporous TiO_2 are the sample crystallinity, pore size and relative anatase content. The highest quantum yield of hydrogen, 0.38, was achieved in the presence of TiO_2(175;500).

3.2.2. Effect of the nature of metal-catalyst upon the quantum yield of hydrogen evolution

Fig. 4 presents kinetic curves of the photocatalytic hydrogen evolution in the presence of the TiO_2(175;500) suspended in water–ethanol mixtures containing $CuCl_2$ (curve 1), Pd/SiO_2 (curve 2), $NiCl_2$ (curve 3) and $AgNO_3$ (curve 4).

The quantum efficiency of hydrogen production increases from Cu to Ni to Ag, catalytic activity of the photodeposited copper nanoparticles being equal to that of Pd/SiO_2. Other metals (Co, Cd, Zn, Fe, Pb) also photocatalytically deposited onto the surface of mesoporous TiO_2, demonstrated negligible activity in catalyzing the photocatalytic hydrogen evolution. In such systems, the quantum yield of the photoreaction does not exceed 10^{-4}. The similar results were obtained with TiO_2 Degussa P25. From the fact it can be speculated that the relative activity of the metals under study does not depend on certain specific properties of the mesoporous titania synthesized in the present study, but reflects more general features of the electronic interaction between the photodeposited metals and the surface of titanium dioxide.

It should be also mentioned that the metal activity growth does not correlate with decrease of the water reduction overvoltage for the corresponding bulk metal electrodes ($Pb \gg Ag > Fe > Cu > Ni \approx Co$) [94]. This means that the catalytic activity of the metal nanoparticles photodeposited onto TiO_2 surface depends not only on their capability of accelerating some "dark" stages of the photocatalytic process (in particular, recombination of the H atoms or hydrogen desorption from the surface of the photocatalyst) but also on some additional specific factors, such as affinity of the metal ions to the surface of titania, size and surface structure of the photodeposited metal nanoparticles and physical characteristics of the contact between the metal and the semiconductor.

The electronic interactions in TiO_2–Cu_n^0 and TiO_2–Ag_n^0 contacts, which were extensively studied in [93,95] by the method of electroreflection both for photocatalytically and electrochemically produced metal nanoparticles showed that copper clusters interact much stronger with the surface of low-doped TiO_2 as compared with silver clusters. These studies demonstrated that the surface states associated with TiO_2–Ag_n^0 electronic contact lie in the band gap of titanium dioxide 2.6–2.7 eV above the top of the valence band (E_{VB}). At the same time, the surface states associated with copper clusters are much deeper—at 2.1–2.2 eV above E_{VB}, which evidences stronger interaction between the semiconductor and metal. Higher electronic affinity of copper clusters to the surface of titanium dioxide as compared to silver was also reported in [96], in the study of TiO_2–metal systems using XPS technique.

Intimate electronic interactions between the copper nanoparticles and TiO_2 surface result in higher rate of metal deposition in the comparison with other metals. It was shown in [97] that the potential of the current growth at the cathodic reduction of a metal on the surface of low-doped TiO_2 shifts to more negative values in the sequence Cu-Cd-Sn-Pb-Pd-Ni-Ag-Pt. The series does not correlate with the redox-potentials of the metals and reflects, probably, relative depth of the surface states localized at TiO_2-metal contact.

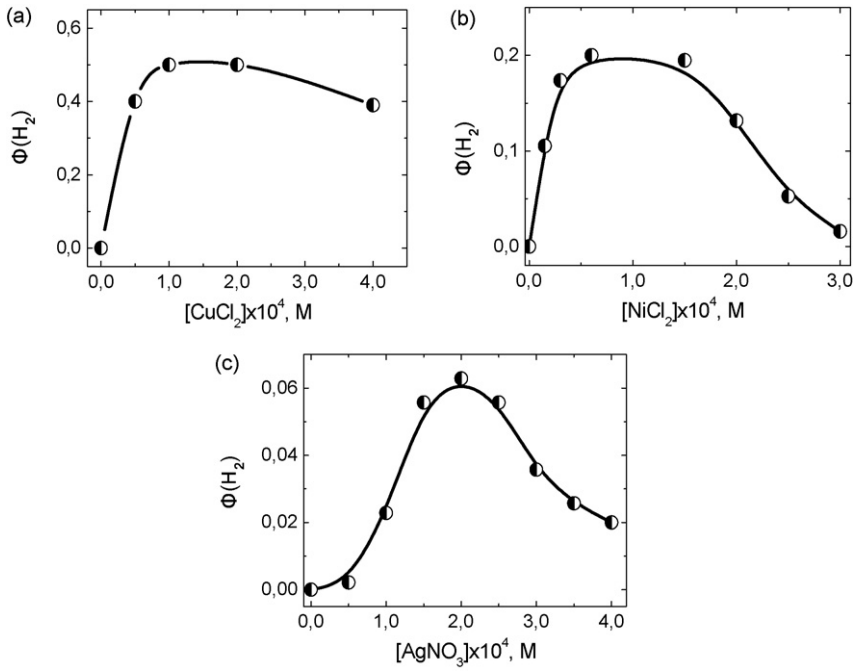

Fig. 5. Dependences between the quantum yield of hydrogen photoproduction from a water–ethanol mixture containing *meso*-TiO_2/Cu_n^0 (a), *meso*-TiO_2/Ni_n^0 (b) and *meso*-TiO_2/Ag_n^0 (c) and the molar metal concentration. Photocatalyst—TiO_2(175;350), 40 °C, $I = 7 \times 10^{-6}$ Einstein/min.

In view of these facts the increase of the quantum yield of the photocatalytic H_2 evolution from TiO_2/Ag_n^0 to TiO_2/Ni_n^0 to TiO_2/Cu_n^0 can be associated with enhancement of the electronic interaction between the photodeposited metal nanoparticles and the surface of titanium dioxide. More advantageous energetics of TiO_2–Cu_n^0 contacts, as compared with other TiO_2–metal systems, favors apparently to more efficient capture of the photogenerated conduction band electrons by surface states and their transfer to metal nanoparticles. This, in turn, suppresses recombination processes with participation of e_{CB}^- and accelerates the total photocatalytic reaction.

3.2.3. *Effect of the metal concentration upon the quantum yield of the photocatalytic hydrogen evolution*

Fig. 5 presents dependences of the quantum yield of the photocatalytic hydrogen evolution, $\Phi(H_2)$, in the presence of *meso*-TiO_2/Cu_n^0, *meso*-TiO_2/Ni_n^0 and meso-TiO_2/Ag_n^0 vs. the initial metal concentration. In case of copper, $\Phi(H_2)$ achieves 0.5 (100% light conversion into hydrogen!) already at $[CuCl_2] = 1.0 \times 10^{-4}$ M and slightly decreases at further increase in Cu^{II} concentration.

Somewhat different tendency was observed in Ni^{II} and Ag^{I}-containing systems. Here, the quantum yield of the photoreaction increases, reaches maximal value at $(0.5–1.5) \times 10^{-4}$ M for Ni^{II} (0.2) and 2.0×10^{-4} M for Ag^{I} (0.07) and lowers drastically with further metal content increase to $(3.0–4.0) \times 10^{-4}$ M.

According to literature data regarding TiO_2-based metal–semiconductor composites with Pt and Rh [1,2,98], Pd [1,3], Ag [1,99] and Ni [69] the observed dependences between the metal content and the photocatalytic process efficiency are quite typical. For example, the maximal photoactivity of the most widely studied TiO_2/Pt composites is usually achieved at 0.5–1.0% metal content and decreases substantially at higher Pt concentration [1,2,98]. Among the possible reasons under the decrease of the quantum yield of the photocatalytic hydrogen production in the systems under investigation could be (i) light filtration by the deposited metal; (ii) partial blockage of TiO_2 surface sites active in the oxidative branch of the photoprocess; (iii) deterioration of the catalytic properties of metal nanoparticles at their enlargement.

Analysis of the dependences presented in Fig. 5 excludes light filtration as a substantial reason for $\Phi(H_2)$ reduction at the metal

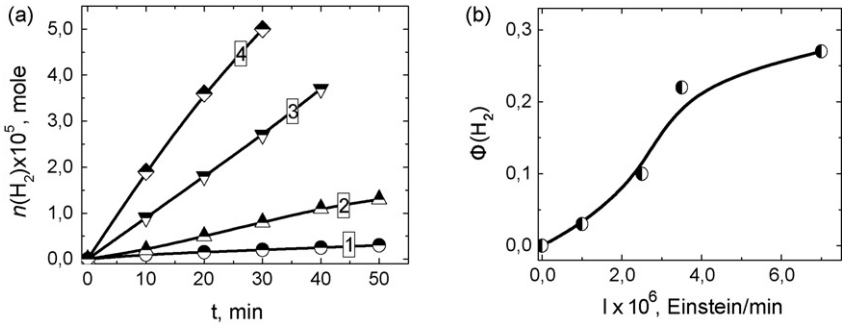

Fig. 6. (a) Kinetic curves of the photocatalytic hydrogen evolution from a water–ethanol mixture containing the *meso*-TiO_2/Cu_n^0 nanocomposite at the light intensity 1.0×10^{-6} (1), 2.5×10^{-6} (2), 3.5×10^{-6} (3) and 7.0×10^{-6} Einstein/min. Photocatalyst—TiO_2(175;350), $[CuCl_2] = 2 \times 10^{-4}$ M, 40 °C. (b) The quantum yield of the hydrogen photoproduction over *meso*-TiO_2/Cu_n^0 vs. light intensity.

content increase. Indeed, the figure shows that the quantum yield of the photoreaction remains quite constant at the metals content variation within a wide range of 1×10^{-4} to 2×10^{-4} M in case of copper and from 0.5×10^{-4} to 1.5×10^{-4} M in case of nickel, while light absorption by the *meso*-TiO_2/Cu_n^0 and *meso*-TiO_2/Ni_n^0 nanocomposites increases drastically. The blockage of the surface sites responsible for the alcohol oxidation h_{VB}^+ could also be dismissed as insignificant since otherwise one should expect oxidation of the photodeposited metals by the photogenerated valence band holes (as is the case in the systems TiO_2-Au [100] and ZnS-Au [101]) with the dissolution of a metal and emptying of the photocatalyst surface. In view of the above discussion one can suggest that the main cause of $\Phi(H_2)$ reduction at the increase in Ni or Ag content is the nanoparticles size growth resulting in deterioration of the electronic contact between the metal nanoparticles and TiO_2 surface with consequent decrease of the charge transfer rate.

It was shown in [93] that the rate of the charge transfer from titanium dioxide to surface states associated with deposited Ag, Pd or Pt nanoparticles lowers at the increase in the metal particles size from 1 to 5 nm, while at the size greater than 5 nm surface states in the band gap of TiO_2 mediating the charge transfer disappear entirely. In case of copper, having stronger affinity to the TiO_2 surface as compared to other metal under discussion, the growth of the nanoparticles size caused by the increase in copper chloride content does not affect substantially the properties of the surface metal–semiconductor contact, thus allowing the photocatalytic activity of the nanostructures *meso*-TiO_2/Cu_n^0 remain steadily high in a wide range of the metal concentrations.

3.2.4. Effect of conditions of the photocatalytic process on its quantum yield

It was found that the intensification of illumination of reacting mixtures results in an increase in the rate of both the photocatalytic metal deposition and the photocatalytic hydrogen evolution. Fig. 6a presents kinetic curves of H_2 formation at variation of the illumination intensity, while Fig. 6b shows the corresponding change in the quantum yield of the photoprocess. A deviation of the latter dependence from linearity towards lower values at comparatively low illumination intensities can be associated with competition between Cu^{II} and water for the photogenerated conduction band electrons. At higher light flows the metal photoreduction finishes already at early stages of the photoprocess and the quantum yield of hydrogen formation tends to a certain constant value independent of the light intensity.

Similar results were obtained for the systems based on *meso*-TiO_2/Ni_n^0, where $\Phi(H_2)$ changes only slightly in a wide range of the illumination intensities. Only 20% decrease in the quantum yield of the photocatalytic hydrogen formation (from 0.38 to 0.31) was observed in the presence of TiO_2(175;500) and $[NiCl_2] = 1.0 \times 10^{-4}$ M at four-times increase in the light intensity—from 0.6 to 2.4×10^{-6} Einstein/min. The observed lowering of $\Phi(H_2)$ with increasing illumination intensity can be accounted for by the non-linear growth of the probability of electron–hole recombination in the semiconductor photocatalyst.

It has been reported earlier [91] that a substantial $\Phi(H_2)$ lowering, from 1.0 to 0.4–0.5 at the increase in the light intensity from 0.6×10^{-6} to 2.4×10^{-6} Einstein/min is observed in the photocatalytic systems for hydrogen evolution based on TiO_2(175;350) and TiO_2(175;500) with Pd/SiO_2. In such systems the co-catalyst deposited on the separate carrier could contact exclusively with the outer surface of the mesoporous TiO_2 and had, therefore, limited capability to capture e_{CB}^- and suppress the electron–hole recombination. In the systems making the subject of this study, the metal deposition evidently takes place both on the outer surface and in the pores of the photocatalyst, which results in more effective capturing of the conduction band electrons by M_n^0 nanoparticles in a wide range of the light intensity.

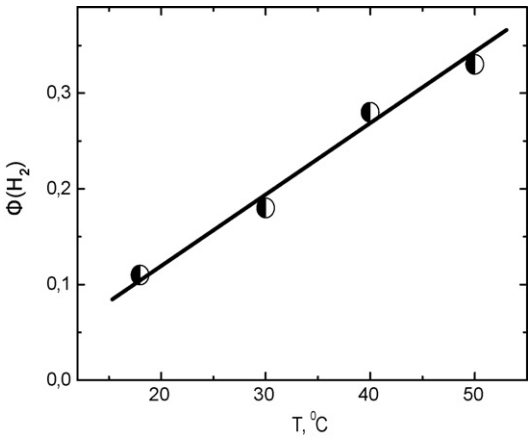

Fig. 7. The quantum yield of the photocatalytic hydrogen production in the presence of *meso*-TiO_2/Cu_n^0 nanocomposite vs. temperature. Photocatalyst—TiO_2(175;350), $[CuCl_2] = 2 \times 10^{-4}$ M, $I = 1.3 \times 10^{-6}$ Einstein/min.

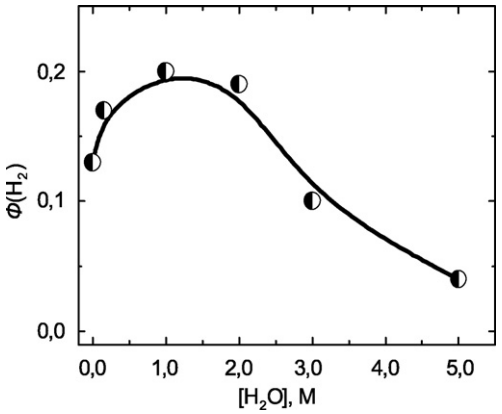

Fig. 8. Dependence between the quantum yield of the photocatalytic hydrogen evolution in the presence of *meso*-TiO_2/Ni_n^0 nanocomposite and the water concentration. Photocatalyst—TiO_2(175;500), $[NiCl_2] = 1 \times 10^{-4}$ M, 20 °C, $I = 1.3 \times 10^{-6}$ Einstein/min.

The quantum yield of the photocatalytic hydrogen production in the presence of TiO_2(175;350)/Cu_n^0 nanocomposites was found to grow from 0.12 to 0.38 at solution temperature increase from 18 to 50 °C (Fig. 7). The dependence presented in the figure cannot be fitted with the Arrhenius equation, its slope being too small for a chemical process requiring substantial thermal activation. An analogy can be drawn with the photocatalytic hydrogen evolution in the presence of zinc sulfide, where poor temperature dependence of the quantum yield was interpreted [93] in terms of the thermal activation of the oxidized electron donor desorption and adsorption of new portions of a donor on the surface of the semiconductor photocatalyst. In our systems, temperature dependences of $\Phi(H_2)$ can similarly originate from thermal activation of acetaldehyde desorption from the TiO_2 surface, which makes it accessible for ethanol molecules, thus contributing to acceleration of the photoreaction.

It was found that the dependence between the quantum yield of the photocatalytic hydrogen formation and the water content is not monotonous and has a maximum at $[H_2O] = 1.0$–2.0 M (Fig. 8). A similar behavior is often observed in the semiconductor-based photocatalytic systems when water–ethanol mixtures [102] are used as a reaction medium instead of dry alcohol, the effect being

due to more favourable water reduction by e_{CB}^- as compared with CH_3CH_2OH molecule reduction [1,102]. The $\Phi(H_2)$ gradually grows in the presence of water with involvement of water molecules involvement into the photocatalytic process and reaches maximum at $[H_2O] = 1.0–2.0$ M. Any further increase of the content of water, which has greater affinity to the TiO_2 surface than ethanol [1,2], results apparently in oversaturation of the photocatalyst surface with H_2O forcing out the ethanol molecules and suppressing their oxidation by the h_{VB}^+.

4. Conclusions

A new template—Na^+ complex with the dibenzo-18-crown-6 was proposed for synthesis of the mesoporous titanium dioxide. It was shown that combination of the hydrothermal treatment of amorphous TiO_2 at 100 or 175 °C with its calcination at 350 or 500 °C results in the formation of the mesoporous titania with specific surface area 130–140 m^2/g, pore diameter 5–9 nm and anatase content 70–90%.

The mesoporous TiO_2 was found to have remarkable photocatalytic activity in reduction of Cu^{II}, Ni^{II} and Ag^{I} ions in water–alcohol mixtures, while the mesoporous metal–semiconductor nanostructures TiO_2/Cu_n^0, TiO_2/Ni_n^0 and TiO_2/Ag_n^0, produced by this reaction, can be used as the photocatalysts of hydrogen evolution. The anatase content and pore size of the mesoporous TiO_2 were found to be the most crucial parameters, affecting the quantum yield of the photocatalytic hydrogen production. The best results were obtained with the sample prepared by the hydrothermal treatment at 175 °C and calcination at 500 °C. The quantum yields of the photocatalytic hydrogen evolution with this sample were found to be 50–60% greater than those observed for TiO_2 Degussa P25.

The rate of the photocatalytic hydrogen formation in water–ethanol mixtures was found to depend strongly on the metal nature, increasing from silver to nickel to copper. This dependence was interpreted in terms of different electronic interactions between metal nanoparticles and TiO_2 surface. It was found that there exists an optimal metal concentration, which gives the maximal quantum yield of the photocatalytic hydrogen formation. A decrease in the photocatalytic activity of *meso*-TiO_2/Ni_n^0 and *meso*-TiO_2/Ag_n^0 at metal concentration higher than optimal was associated with deterioration of the electronic interactions between the components of metal–semiconductor composites with growth of the metal nanoparticles size.

The quantum yield of the photocatalytic hydrogen evolution was found to remain constant within the large range of the illumination intensity variation. An increase in the rate of the photocatalytic reaction with temperature elevation was attributed to thermal activation of the desorption of ethanol oxidation products from the photocatalyst surface. An extremal dependence between the quantum yield of the photocatalytic hydrogen formation and the water content was interpreted in terms of the competitive adsorption of water and alcohol on the surface of mesoporous TiO_2.

It should be noted that along with the obvious advantages of the photocatalytic systems studied in the present work, which consist in high efficiency of light-to-hydrogen conversion and unnecessity of the utilization of a noble metal as a co-catalyst (as is usually the case for the TiO_2-based photocatalytic systems), they have also certain shortcomings. The most serious among them is the low sensitivity of the mesoporous TiO_2 to the visible light. In this view, the research is under way aimed at the spectral sensitization of the mesoporous TiO_2 with organic dyes and narrow band gap semiconductors, such as CdS and Bi_2S_3. The results of this research will be published separately.

References

[1] M. Grätzel (Ed.), Energy Resources through Photochemistry and Catalysis, Academic Press, New York, 1983.
[2] A. Hagfeldt, M. Grätzel, Chem. Rev. 95 (1995) 49.
[3] A. Fujishima, T.N. Rao, D.A. Tryk, Photochem. Photobiol. C 1 (2000) 1.
[4] N. Serpone, D. Lawless, R.F. Khairutdinov, J. Phys. Chem. 99 (1995) 16655.
[5] H.-D. Jang, S.-K. Kim, S.-J. Kim, J. Nanoparticles Res. 3 (2001) 141.
[6] K. Rajeshwar, C.R. Chenthamarakshan, S. Goeringer, M. Djukic, Pure Appl. Chem. 73 (2001) 1849.
[7] M. Fernández-García, A. Martínez-Arias, J.C. Hanson, J.A. Rodriguez, Chem. Rev. 104 (2004) 4063.
[8] X. Chen, S.S. Mao, Chem. Rev. 107 (2007) 2891.
[9] M. Grätzel, J. Photochem. Photobiol. C 4 (2003) 145.
[10] C. Yu, B. Tian, D. Zhao, Curr. Opin. Solid State Mater. Sci. 7 (2003) 191.
[11] D.G. Shchukin, D.V. Sviridov, J. Photochem. Photobiol. C 7 (2006) 23.
[12] D.V. Bavykin, J.M. Friedrich, F.C. Walsch, Adv. Mater. 18 (2006) 2807.
[13] G.J. Soler-Illia, C. Sanchez, B. Lebeau, J. Patarin, Chem. Rev. 102 (2002) 4093.
[14] Y.K. Hwang, K.-C. Lee, Y.-U. Kwon, Chem. Commun. (2001) 1738.
[15] Y. Yue, Z. Gao, Chem. Commun. (2000) 1755.
[16] D. Grosso, G.J. Soler-Illia, F. Babonneau, C. Sanchez, P.-A. Albouy, A. Brunet-Bruneau, A.R. Balkenende, Adv. Mater. 13 (2001) 1085.
[17] P. Yang, D. Zhao, D.I. Margolese, B.F. Chmelka, G.D. Stucky, Chem. Mater. 11 (1999) 2813.
[18] B.L. Kirsch, E.K. Richman, A.E. Riley, S.H. Tolbert, J. Phys. Chem. B 108 (2004) 12698.
[19] T.-Z. Ren, Z.-Y. Yuan, B.-L. Su, Colloids Surf. A 241 (2004) 67.
[20] L. Kavan, J. Rathouský, M. Grätzel, V. Shklover, A. Zukal, Microporous Mesoporous Mater. 44–45 (2001) 653.
[21] S. Eiden-Assmann, J. Widoniak, G. Maret, Chem. Mater. 16 (2004) 6.
[22] N. Bao, K. Yanagisawa, X. Lu, X. Feng, Chem. Lett. 33 (2004) 346.
[23] J. Yu, J.C. Yu, W. Ho, Z. Jiang, New J. Chem. 26 (2002) 607.
[24] Y. Sakatani, D. Grosso, L. Nicole, C. Boissière, G.J. Soler-Illia, C. Sanchez, J. Mater. Chem. 16 (2006) 77.
[25] S. Zhan, D. Chen, X. Jiao, C. Tao, J. Phys. Chem. B 110 (2006) 11199.
[26] M. Alvaro, C. Aprile, M. Benitez, E. Carbonell, H. Garcia, J. Phys. Chem. B 110 (2006) 6661.
[27] J.N. Kondo, T. Yamashita, K. Nakajima, D. Lu, M. Hara, K. Domen, J. Mater. Chem. 15 (2005) 2035.
[28] M. Wark, J. Tschirch, O. Bartels, D. Bahnemann, J. Rathouský, Microporous Mesoporous Mater. 84 (2005) 247.
[29] J. Tang, Y. Wu, E.W. McFarland, G.D. Stucky, Chem. Commun. (2004) 1670.
[30] J.H. Schattka, D.G. Shchukin, J. Jia, M. Antonietti, R.A. Caruso, Chem. Mater. 14 (2002) 5103.
[31] C. Wang, H. Xi, R.-D. Wang, Chem. Lett. 33 (2004) 20.
[32] T.N. Murakami, H. Saito, S. Uegusa, N. Kawashima, T. Miyasaka, Chem. Lett. 32 (2003) 1154.
[33] B. Guo, Z. Liu, L. Hong, X. Jiang, Surf. Coat. Technol. 198 (2005) 24.
[34] G. Wittmann, K. Demeestere, A. Dombi, J. Dewulf, H. van Langenhove, Appl. Catal. B 61 (2005) 47.
[35] T.M. Salama, I.O. Ali, M.M. Mohamed, J. Mol. Catal. A 273 (2007) 198.
[36] S. Ikeda, I. Ikoma, H. Kobayashi, et al., Chem. Commun. (2007) 3753.
[37] Z. Liu, Z. Jin, X. Liu, Y. Fu, G. Liu, J. Sol-Gel Sci. Technol. 38 (2006) 73.
[38] K. Cassiers, T. Linssen, M. Mathieu, Y.Q. Bai, H.Y. Zhu, P. Cool, E.F. Vansant, J. Phys. Chem. B 108 (2004) 3713.
[39] E. Beyers, P. Cool, E.F. Vansant, J. Phys. Chem. B 109 (2005) 10081.
[40] X. Zhang, F. Zhang, K.-Y. Chan, Appl. Catal. A 284 (2005) 193.
[41] T. Peng, D. Zhao, K. Dai, W. Shi, K. Hirao, J. Phys. Chem. B 109 (2005) 4947.
[42] Q. Dai, L.Y. Shi, Y.G. Luo, J.L. Blin, D.J. Li, C.W. Yuan, B.L. Su, J. Photochem. Photobiol. A 148 (2002) 295.
[43] A.K. Sinha, K. Suzuki, J. Phys. Chem. B 109 (2005) 1708.
[44] E. Beyers, P.E.F. Cool, Microporous Mesoporous Mater. 99 (2007) 112.
[45] M.P. Kapoor, S. Inagaki, H. Yoshida, J. Phys. Chem. B 109 (2005) 9231.
[46] K. Cassiers, T. Linssen, V. Meyner, P. Van Der Voort, P. Cool, E.F. Vansant, Chem. Commun. (2003) 1178.
[47] E.A. Kozlova, A.V. Vorontsov, Appl. Catal. B 77 (2007) 35.
[48] H. Choi, M.G. Antoniou, M. Pelaez, et al., Environ. Sci. Technol. 41 (2007) 7530.
[49] V.F. Stone Jr., R.J. Davis, Chem. Mater. 10 (1998) 1468.
[50] J.C. Yu, J. Yu, J. Zhao, Appl. Catal. B 36 (2002) 31.
[51] J.C. Yu, J. Yu, W. Ho, J. Zhao, J. Photochem. Photobiol. A 148 (2002) 331.
[52] M. Yan, F. Chen, J. Zhang, M. Anpo, J. Phys. Chem. B 109 (2005) 8673.
[53] S. Pavasupree, J. Jitputti, S. Ngamsinlapasathian, S. Yoshikawa, Mater. Res. Bull. 43 (2008) 149.
[54] K. Liu, H. Fu, K. Shi, F. Xiao, L. Jing, B. Xin, J. Phys. Chem. B 109 (2005) 18719.
[55] D.S. Kim, S.-Y. Kwak, Appl. Catal. A 323 (2007) 110.
[56] M.A. Carreon, S.Y. Choi, M. Mamak, N. Chopra, G.A. Ozin, J. Mater. Chem. 17 (2007) 82.
[57] K. Wang, B. Yao, M.A. Morris, J.D. Holmes, Chem. Mater. 17 (2005) 4825.
[58] P.C. Angelomé, L. Andrini, M.E. Calvo, et al., J. Phys. Chem. C 111 (2007) 10886.
[59] L. Chen, B. Yao, Y. Cao, K. Fan, J. Phys. Chem. C 111 (2007) 11849.
[60] W. Chen, X. Sun, Q. Cai, D. Weng, H. Li, Electrochem. Commun. 9 (2007) 382.
[61] Y. Ou, J. Lin, S. Fang, D. Liao, Catal. Commun. 8 (2007) 936.
[62] J.C. Yu, L. Zhang, J. Yu, New J. Chem. 26 (2002) 416.
[63] L. Zhang, J.C. Yu, Chem. Commun. (2003) 2078.

[64] Y. Matsumoto, Y. Ishikawa, M. Nishida, S. Ii, J. Phys. Chem. B 104 (2000) 4204.
[65] M. Grätzel, Curr. Opin. Colloid Interface Sci. 4 (1999) 314.
[66] N.-L. Wu, M.-S. Lee, Z.-J. Pon, J.-Z. Hsu, Photochem. Photobiol. A 163 (2004) 277.
[67] T. Sreethawong, Y. Suzuki, S. Yoshikawa, Catal. Commun. 6 (2005) 119.
[68] T. Sreethawong, S. Yoshikawa, Catal. Commun. 6 (2005) 661.
[69] D. Jing, Y. Zhang, L. Guo, Chem. Phys. Lett. 415 (2005) 74.
[70] T. Sreethawong, Y. Suzuki, S. Yoshikawa, J. Solid State Chem. 178 (2005) 329.
[71] X. Wang, J.C. Yu, C. Ho, Y. Hou, X. Fu, Langmuir 21 (2005) 2552.
[72] G. Goutailler, C. Guillard, S. Daniele, L.G. Hubert-Pfalzgraf, J. Mater. Chem. 13 (2003) 342.
[73] J. Yu, L. Zhang, B. Cheng, Y. Su, J. Phys. Chem. C 111 (2007) 10582.
[74] H. Yu, X.-J. Li, S.-J. Zheng, W. Xu, Mater. Chem. Phys. 97 (2006) 59.
[75] Y. Zhang, J. Li, J. Wang, Chem. Mater. 18 (2006) 2917.
[76] Y. Shiraishi, N. Saito, T. Hirai, J. Am. Chem. Soc. 127 (2005) 12820.
[77] M. Wei, Y. Konishi, H. Zhou, M. Yanagida, H. Sugihara, H. Arakawa, J. Mater. Chem. 16 (2006) 1287.
[78] T. Miyao, Y. Suzuki, S. Naito, Catal. Lett. 66 (2000) 197.
[79] C.-H. Lin, C.-H. Lee, J.-H. Chao, C.-Y. Kuo, Y.-C. Cheng, W.-N. Huang, H.-W. Chang, Y.-M. Huang, M.-K. Shih, Catal. Lett. 98 (2004) 61.
[80] A. Yamakata, T. Ishibashi, H. Onishi, J. Mol. Catal. A 199 (2003) 85.
[81] D. Behar, J. Rabani, J. Phys. Chem. B 110 (2006) 8750.
[82] Y. Li, G. Lu, S. Li, J. Photochem. Photobiol. A 152 (2002) 219.
[83] N.-L. Wu, M.-S. Lee, Int. J. Hydrogen Energy 29 (2004) 1601.
[84] K. Byrappa, T. Adschiri, Prog. Cryst. Growth Character. Mater. 53 (2007) 117.
[85] J. Ovenstone, K. Yanagisawa, Chem. Mater. 11 (1999) 2770.
[86] K. Yanagisawa, J. Ovenstone, J. Phys. Chem. B 103 (1999) 7781.
[87] V.N. Kuznetsov, T.K. Krutitskaya, Kinetics Catal. (Russ. Ed.) 37 (1996) 472.
[88] G. Lu, A. Linsebigler, J.T. Yates Jr., J. Phys. Chem. 98 (1994) 11733.
[89] H. Wang, J. He, G. Boschloo, H. Lindström, A. Hagfeldt, S.-E. Lindquist, J. Phys. Chem. B 105 (2001) 2529.
[90] G. Boschloo, D. Fitzmaurice, J. Phys. Chem. B 103 (1999) 2228.
[91] V.I. Yatskiv, A.V. Korzhak, V.M. Granchak, A.S. Kovalenko, S.Ya. Kuchmiy, Theor. Exp. Chem. 39 (2003) 167.
[92] F. Forouzan, T.C. Richards, A.J. Bard, J. Phys. Chem. 100 (1996) 18123.
[93] A.I. Kulak, Electrochemistry of Semiconductor Heterostrucrures (In Russ.), Universitetskoye, Minsk, 1986.
[94] L.I. Antropov, Theoretical Electrochemistry (In Russ.), Vysshaya shkola, Moscow, 1965.
[95] E.A. Streltsov, R.M. Lazorenko-Manevich, V.P. Pakhomov, A.I. Kulak, Electrochemistry (Russ. Ed) 19 (1983) 1148.
[96] U. Diebold, Surf. Sci. Rep. 48 (2003) 53.
[97] E.A. Streltsov, V.V. Sviridov, A.I. Kulak, V.P. Pakhomov, Electrochemistry (Russ. Ed.) 19 (1983) 1000.
[98] A.V. Vorontsov, I.V. Stoyanova, D.V. Kozlov, V.I. Simagina, E.I. Savinov, J. Catal. 189 (2000) 360.
[99] B. Ohtani, S. Nishimoto, J. Phys. Chem. 97 (1993) 920.
[100] V. Subramanian, E. Wolf, P.V. Kamat, J. Phys. Chem. B 105 (2001) 11439.
[101] A.L. Stroyuk, A.E. Raevskaya, A.V. Korzhak, S.Ya. Kuchmiy, J. Nanoparticle Res. 9 (2007) 1027.
[102] A.I. Kryukov, S.Ya. Kuchmiy, V.D. Pokhodenko, Theor. Exp. Chem. 33 (1997) 306.